EUROPEAN ORGANISATION FOR NUCLEAR RESEARCH

CERN-PPE/95-13
3 February 1995

Comparisons of the Properties of Final State Photons in Hadronic Z^0 Decays with Predictions from Matrix Element Calculations

The OPAL Collaboration

Abstract

The properties of hadronic Z^0 decays with final state photons, measured with OPAL at LEP, have been compared with predictions from two different matrix element calculations of $\mathcal{O}(\alpha\alpha_s)$. Two calculations, GNJETS and EEPRAD, have been investigated which use different schemes to restrict the phase space around the poles of the cross section. Assuming the E0-JADE jet definition, both calculations describe the data well in large regions of phase space for y_{cut} values around 0.06. For very large and very small jet-photon masses some deviations from the predictions have been found, indicating the importance of higher order corrections.

Significant differences between the calculations are only apparent in the predicted rate of 1-jet plus photon events. The rate is higher in GNJETS which reproduces the data better than EEPRAD.

To be submitted to Zeitschrift für Physik

The OPAL Collaboration

R. Akers[16], G. Alexander[23], J. Allison[16], K. Ametewee[25], K.J. Anderson[9], S. Arcelli[2], S. Asai[24], D. Axen[29], G. Azuelos[18,a], A.H. Ball[17], E. Barberio[26], R.J. Barlow[16], R. Bartoldus[3], J.R. Batley[5], G. Beaudoin[18], A. Beck[23], G.A. Beck[13], C. Beeston[16], T. Behnke[27], K.W. Bell[20], G. Bella[23], S. Bentvelsen[8], P. Berlich[10], S. Bethke[32], O. Biebel[32], I.J. Bloodworth[1], P. Bock[11], H.M. Bosch[11], M. Boutemeur[18], S. Braibant[12], P. Bright-Thomas[25], R.M. Brown[20], A. Buijs[8], H.J. Burckhart[8], R. Bürgin[10], C. Burgard[27], N. Capdevielle[18], P. Capiluppi[2], R.K. Carnegie[6], A.A. Carter[13], J.R. Carter[5], C.Y. Chang[17], C. Charlesworth[6], D.G. Charlton[1,b], S.L. Chu[4], P.E.L. Clarke[15], J.C. Clayton[1], S.G. Clowes[16], I. Cohen[23], J.E. Conboy[15], O.C. Cooke[16], M. Cuffiani[2], S. Dado[22], C. Dallapiccola[17], G.M. Dallavalle[2], C. Darling[31], S. De Jong[12], L.A. del Pozo[8], H. Deng[17], M. Dittmar[4], M.S. Dixit[7], E. do Couto e Silva[12], J.E. Duboscq[8], E. Duchovni[26], G. Duckeck[8], I.P. Duerdoth[16], U.C. Dunwoody[5], J.E.G. Edwards[16], P.A. Elcombe[5], P.G. Estabrooks[6], E. Etzion[23], H.G. Evans[9], F. Fabbri[2], B. Fabbro[21], M. Fanti[2], P. Fath[11], M. Fierro[2], M. Fincke-Keeler[28], H.M. Fischer[3], P. Fischer[3], R. Folman[26], D.G. Fong[17], M. Foucher[17], H. Fukui[24], A. Fürtjes[8], P. Gagnon[6], A. Gaidot[21], J.W. Gary[4], J. Gascon[18], N.I. Geddes[20], C. Geich-Gimbel[3], S.W. Gensler[9], F.X. Gentit[21], T. Geralis[20], G. Giacomelli[2], P. Giacomelli[4], R. Giacomelli[2], V. Gibson[5], W.R. Gibson[13], J.D. Gillies[20], J. Goldberg[22], D.M. Gingrich[30,a], M.J. Goodrick[5], W. Gorn[4], C. Grandi[2], E. Gross[26], J. Hagemann[27], G.G. Hanson[12], M. Hansroul[8], C.K. Hargrove[7], P.A. Hart[9], M. Hauschild[8], C.M. Hawkes[8], E. Heflin[4], R.J. Hemingway[6], G. Herten[10], R.D. Heuer[8], J.C. Hill[5], S.J. Hillier[8], T. Hilse[10], P.R. Hobson[25], D. Hochman[26], R.J. Homer[1], A.K. Honma[28,a], R. Howard[29], R.E. Hughes-Jones[16], P. Igo-Kemenes[11], D.C. Imrie[25], A. Jawahery[17], P.W. Jeffreys[20], H. Jeremie[18], M. Jimack[1], M. Jones[6], R.W.L. Jones[8], P. Jovanovic[1], C. Jui[4], D. Karlen[6], J. Kanzaki[24], K. Kawagoe[24], T. Kawamoto[24], R.K. Keeler[28], R.G. Kellogg[17], B.W. Kennedy[20], B. King[8], J. King[13], J. Kirk[29], S. Kluth[5], T. Kobayashi[24], M. Kobel[10], D.S. Koetke[6], T.P. Kokott[3], S. Komamiya[24], R. Kowalewski[8], T. Kress[11], P. Krieger[6], J. von Krogh[11], P. Kyberd[13], G.D. Lafferty[16], H. Lafoux[8], R. Lahmann[17], W.P. Lai[19], J. Lauber[8], J.G. Layter[4], P. Leblanc[18], A.M. Lee[31], E. Lefebvre[18], D. Lellouch[26], C. Leroy[18], J. Letts[2], L. Levinson[26], S.L. Lloyd[13], F.K. Loebinger[16], G.D. Long[17], B. Lorazo[18], M.J. Losty[7], X.C. Lou[8], J. Ludwig[10], A. Luig[10], M. Mannelli[8], S. Marcellini[2], C. Markus[3], A.J. Martin[13], J.P. Martin[18], T. Mashimo[24], W. Matthews[25], P. Mättig[3], U. Maur[3], J. McKenna[29], T.J. McMahon[1], A.I. McNab[13], F. Meijers[8], F.S. Merritt[9], H. Mes[7], A. Michelini[8], R.P. Middleton[20], G. Mikenberg[26], D.J. Miller[15], R. Mir[26], W. Mohr[10], A. Montanari[2], T. Mori[24], M. Morii[24], U. Müller[3], B. Nellen[3], B. Nijjhar[16], S.W. O'Neale[1], F.G. Oakham[7], F. Odorici[2], H.O. Ogren[12], N.J. Oldershaw[16], C.J. Oram[28,a], M.J. Oreglia[9], S. Orito[24], F. Palmonari[2], J.P. Pansart[21], G.N. Patrick[20], M.J. Pearce[1], P.D. Phillips[16], J.E. Pilcher[9], J. Pinfold[30], D.E. Plane[8], P. Poffenberger[28], B. Poli[2], A. Posthaus[3], T.W. Pritchard[13], H. Przysiezniak[30], M.W. Redmond[8], D.L. Rees[8], D. Rigby[1], M.G. Rison[5], S.A. Robins[13], D. Robinson[5], N. Rodning[30], J.M. Roney[28], E. Ros[8], A.M. Rossi[2], M. Rosvick[28], P. Routenburg[30], Y. Rozen[8], K. Runge[10], O. Runolfsson[8], D.R. Rust[12], M. Sasaki[24], C. Sbarra[2], A.D. Schaile[8], O. Schaile[10], F. Scharf[3], P. Scharff-Hansen[8], P. Schenk[4], B. Schmitt[3], M. Schröder[8], H.C. Schultz-Coulon[10], P. Schütz[3], M. Schulz[8], C. Schwick[27], J. Schwiening[3], W.G. Scott[20], M. Settles[12], T.G. Shears[5], B.C. Shen[4], C.H. Shepherd-Themistocleous[7], P. Sherwood[15], G.P. Siroli[2], A. Skillman[15], A. Skuja[17], A.M. Smith[8], T.J. Smith[28], G.A. Snow[17], R. Sobie[28], S. Söldner-Rembold[10], R.W. Springer[30], M. Sproston[20], A. Stahl[3], J. Stamm[3] M. Starks[12], C. Stegmann[10], K. Stephens[16], J. Steuerer[28], B. Stockhausen[3], D. Strom[19], P. Szymanski[20], R. Tafirout[18],

H. Takeda[24], T. Takeshita[24], P. Taras[18], S. Tarem[26], M. Tecchio[9], P. Teixeira-Dias[11], N. Tesch[3], M.A. Thomson[8], O. Tousignant[18], S. Towers[6], M. Tscheulin[10], T. Tsukamoto[24], A.S. Turcot[9], M.F. Turner-Watson[8], P. Utzat[11], R. Van Kooten[12], G. Vasseur[21], P. Vikas[18], M. Vincter[28], A. Wagner[27], D.L. Wagner[9], C.P. Ward[5], D.R. Ward[5], J.J. Ward[15], P.M. Watkins[1], A.T. Watson[1], N.K. Watson[7], P. Weber[6], P.S. Wells[8], N. Wermes[3], B. Wilkens[10], G.W. Wilson[27], J.A. Wilson[1], V-H. Winterer[10], T. Wlodek[26], G. Wolf[26], S. Wotton[11], T.R. Wyatt[16], A. Yeaman[13], G. Yekutieli[26], M. Yurko[18], V. Zacek[18], W. Zeuner[8], G.T. Zorn[17].

[1]School of Physics and Space Research, University of Birmingham, Birmingham B15 2TT, UK
[2]Dipartimento di Fisica dell' Università di Bologna and INFN, I-40126 Bologna, Italy
[3]Physikalisches Institut, Universität Bonn, D-53115 Bonn, Germany
[4]Department of Physics, University of California, Riverside CA 92521, USA
[5]Cavendish Laboratory, Cambridge CB3 0HE, UK
[6]Carleton University, Department of Physics, Colonel By Drive, Ottawa, Ontario K1S 5B6, Canada
[7]Centre for Research in Particle Physics, Carleton University, Ottawa, Ontario K1S 5B6, Canada
[8]CERN, European Organisation for Particle Physics, CH-1211 Geneva 23, Switzerland
[9]Enrico Fermi Institute and Department of Physics, University of Chicago, Chicago IL 60637, USA
[10]Fakultät für Physik, Albert Ludwigs Universität, D-79104 Freiburg, Germany
[11]Physikalisches Institut, Universität Heidelberg, D-69120 Heidelberg, Germany
[12]Indiana University, Department of Physics, Swain Hall West 117, Bloomington IN 47405, USA
[13]Queen Mary and Westfield College, University of London, London E1 4NS, UK
[15]University College London, London WC1E 6BT, UK
[16]Department of Physics, Schuster Laboratory, The University, Manchester M13 9PL, UK
[17]Department of Physics, University of Maryland, College Park, MD 20742, USA
[18]Laboratoire de Physique Nucléaire, Université de Montréal, Montréal, Quebec H3C 3J7, Canada
[19]University of Oregon, Department of Physics, Eugene OR 97403, USA
[20]Rutherford Appleton Laboratory, Chilton, Didcot, Oxfordshire OX11 0QX, UK
[21]CEA, DAPNIA/SPP, CE-Saclay, F-91191 Gif-sur-Yvette, France
[22]Department of Physics, Technion-Israel Institute of Technology, Haifa 32000, Israel
[23]Department of Physics and Astronomy, Tel Aviv University, Tel Aviv 69978, Israel
[24]International Centre for Elementary Particle Physics and Department of Physics, University of Tokyo, Tokyo 113, and Kobe University, Kobe 657, Japan
[25]Brunel University, Uxbridge, Middlesex UB8 3PH, UK
[26]Particle Physics Department, Weizmann Institute of Science, Rehovot 76100, Israel
[27]Universität Hamburg/DESY, II Institut für Experimental Physik, Notkestrasse 85, D-22607 Hamburg, Germany
[28]University of Victoria, Department of Physics, P O Box 3055, Victoria BC V8W 3P6, Canada
[29]University of British Columbia, Department of Physics, Vancouver BC V6T 1Z1, Canada
[30]University of Alberta, Department of Physics, Edmonton AB T6G 2J1, Canada
[31]Duke University, Dept of Physics, Durham, NC 27708-0305, USA
[32]Technische Hochschule Aachen, III Physikalisches Institut, Sommerfeldstrasse 26-28, D-52056

Aachen, Germany

[a] Also at TRIUMF, Vancouver, Canada V6T 2A3
[b] Royal Society University Research Fellow

1 Introduction

Photon bremsstrahlung from quarks can be used to examine the strength and structure of the strong and electroweak sectors of the standard model [1–6]. These tests, however, require reliable and unambiguous theoretical predictions. Furthermore, final state photons must be considered as background in any search for new phenomena with quarks and photons in the final state, also requiring a reliable prediction of the $q\bar{q}\gamma$ cross section.

QCD shower models are very successful in simulating inclusive hadronic Z^0 decays and they are also able to describe the general event shapes of final state photon events [4,6]. However, their implementation requires several parameters and certain technical assumptions. It has been found that the predictions of the absolute cross section for final state photons differ significantly among the different models [3,4]. The reasons for these differences between the models are still under investigation and therefore their use for precision measurements is limited.

Matrix element calculations describe photon radiation from quarks from the first principles of QED and QCD and do not involve models, but they are unable to describe the detailed properties of events. Recently, matrix element calculations in $\mathcal{O}(\alpha\alpha_s)$ have been evaluated by Monte Carlo methods [7–10], which are compared to a measurement of event properties of final state photon events in this paper. This comparison aims at testing whether these calculations can reproduce the global event configuration and hopes to identify those phase space regions where the lowest order α_s approximation leads to reliable predictions and those where higher order corrections have to be taken into account. The value of the lowest order α_s which gives the best description of the data is used as an indicator to assess the possible importance of higher order QCD corrections.

Compared to previous OPAL investigations of final state photon events [2–5] the endcap region of the detector has been included for photon detection, extending the polar detection limit for photons closer to the beam direction. An improved understanding of the detector and the background allows the requirements on the minimum photon energy and the isolation of the photon in the event selection to be relaxed. This leads to a larger photon acceptance and a reduction of the corrections which, together with the increased statistics, allows a detailed investigation of large phase space regions.

After a short description of the detector components essential for this analysis there follows in sections 3 and 4 a summary of the event selection procedure and the background estimate. In section 5 the correction procedure used to prepare the event sample for a comparison with the matrix element calculations is described. In section 6, the essential features of matrix element Monte Carlos are introduced and the adjustment of their internal parameters restricting the phase space for photon emission is summarised. Results are presented for the comparison of properties of final state photon events with the matrix element predictions in section 7 and some conclusions are drawn in section 8.

2 The OPAL Detector

A detailed description of the OPAL detector can be found elsewhere [11]. Here we only review the central detector and the electromagnetic calorimeter, which are essential for this analysis. The central detector consists of a system of cylindrical tracking chambers surrounded by a solenoidal coil with a uniform magnetic field of 0.435 T. The tracking system provides the measurement of the momenta of charged particles. The detection efficiency for charged particles is almost 100% within the polar angle range $|\cos\theta| < 0.92$ where θ denotes the track angle with respect to the beam direction.

The barrel part of the electromagnetic calorimeter covers the entire azimuth, and the polar angle range $|\cos\theta| < 0.82$. It consists of 9440 lead glass blocks of 24.6 radiation lengths depth, almost pointing towards the interaction region and each subtending an angular region of approximately 40×40 mrad^2. The two endcap calorimeters each consist of 1132 lead glass blocks oriented parallel to the beam axis and of about 22 radiation lengths depth. They cover the polar angle region of $0.82 \leq |\cos\theta| \leq 0.98$. Deposits of energy in adjacent blocks are grouped together to form 'clusters' of electromagnetic energy.

3 The Selection of Events with Final State Photons

The analysis is based on an integrated luminosity of approximately 46 pb^{-1}, collected with the OPAL detector [11] at LEP in 1991 and 1992. The data were recorded at centre-of-mass energies between 88.28 GeV and 94.28 GeV around the Z^0 resonance.

With the requirements used in the OPAL analysis of the electroweak parameters of the Z^0 [12] a sample of 1.12×10^6 hadronic Z^0 decays has been selected with an acceptance, estimated from Monte Carlo studies, of 0.984 ± 0.004. The background fraction from τ pairs and two photon processes was found to be less than 0.003.

The selection of events with final state photons requires a well measured photon candidate. Most of the hadronic background, simulating photons, is expected in the vicinity of jets. Therefore, high energy isolated clusters in the electromagnetic calorimeter have been selected with the following requirements:

- The photon candidate has to be within a fiducial volume of the lead glass calorimeter ($|\cos\theta| < 0.72$ or $0.82 \leq |\cos\theta| \leq 0.92$). The intermediate region $0.72 \leq |\cos\theta| \leq 0.82$ has not been used, as the response of the calorimeters is substantially degraded by the presence of up to 8 radiation lengths of material in front of the lead glass.
- The photon energy has to be larger than 5 GeV.
- No track with a transverse momentum with respect to the beam direction of more than 250 MeV/c or any additional cluster with an electromagnetic energy exceeding 250 MeV is allowed within an isolation cone of half-angle 10 degrees around the flight direction of the photon candidate.

- The photon candidate has to be separated from any jet. To this end, all tracks and clusters in an event except the photon candidate are combined into jets. Jets are constructed by iteratively combining the pair of particles or combinations of particles that have the smallest value of

$$y_{ij} = \frac{M_{ij}^2}{E_{vis}^2}$$

in each iteration. The particles are combined as long as y_{ij} is smaller than a specified value y_{cut}. The quantity M_{ij} is calculated using the JADE E0 scheme [13] with M_{ij}^2 given by $2E_iE_j(1-\cos\alpha_{ij})$, where E_i and E_j are the energies and α_{ij} is the opening angle of these pairs. The visible energy E_{vis} is calculated from all tracks and clusters including the photon candidate.

In a second step $y_{\gamma,jet}$ is calculated by pairing the photon candidate with each jet. At this stage the jet energies and E_{vis} of the event are corrected for double counting of tracks and clusters from the same particle, as described in [14].

An event is accepted if $y_{\gamma,jet}$ of the photon with each jet is larger than the same y_{cut} as used for the jet finding.

- To suppress further background from hadrons, the cluster properties are required to agree with those expected from a single photon. Due to the detector geometry these requirements are different for the barrel and endcap region. For the barrel region the requirements are the same as in [2–5]. Briefly, the number of lead glass blocks per cluster has to be less than 16. The energy weighted width of the cluster has to be smaller than 30 mrad and a cluster shape variable has to have a value consistent with those arising from real photon clusters [3]. These requirements result in a photon detection efficiency of 0.936 $\pm$ 0.016, measured with photons from radiative lepton pairs and two photon production events (for details see [3]). No dependence of the efficiency on the photon energy has been found.

  In the endcap region ($0.82 \leq |\cos\theta| \leq 0.92$) the cluster width has to be smaller than 45 mrad and at least 70% of the cluster energy must be deposited in two blocks. The detection efficiency has been found to be 0.912$\pm$0.020 for photons below 30 GeV and between 0.84 and 0.87 for photon energies above 30 GeV.

Additional losses are due to photon conversions in the central detector. For a photon traversing the detector perpendicular to the beam direction these amount to 6.3$\pm$1.2 %.

For the three y_{cut} values 0.02, 0.06 and 0.2, which will be considered in detail in the following analysis, the number of photon candidates selected was 2857, 1706 and 719, respectively.

4 The Background to the Photon Sample

There are two kinds of background to the direct photon sample: hadronic background mainly from high energy π^0 decays faking a single photon; and photons from initial state radiation. The background from both sources has been determined as described below and has been subtracted for each bin of the studied distributions.

From isospin symmetry it is expected that the number of neutral, positively and negatively charged pions is equal, allowing an estimate of the hadronic background to be made from the data. The strategy is to translate the number of isolated charged tracks in the data into an estimator for the number of neutral hadrons faking a photon. This method has been used in our previous publications [2–5]. A sample of well measured, isolated charged tracks has been selected with the same energy and isolation requirements as for the photon candidates. This sample has been corrected for the selection efficiency and for tracks accompanied by an unresolvable neutral particle. Assuming a charged particle composition of 70% pions, 20% kaons and 10% protons, consistent with [15], and correcting for the rejection probability of the cluster shape variables as a function of the energy, the number of charged particles has been converted into a background from isolated neutral hadrons. To account for the uncertainties in the composition of the charged particle yield and the fraction of decays violating isospin symmetry, a systematic error of 50% has been assigned for this background estimate. For the distributions discussed in this paper the background has been estimated individually for each bin. Typically the hadronic background amounts to 11% of the photon candidates for both the barrel and endcap regions.

The background from initial state radiation has been estimated using the first order QED calculation of [16] as implemented in JETSET 7.3 [17] taking into account the distribution of the centre-of-mass energy of the data. In the barrel region, this background decreases as a function of y_{cut} and varies between 7% and 3% of the photon candidates. In the endcap region, about 15% of the photon candidates are from initial state radiation, independent of y_{cut}.

5 The Acceptance and Hadronisation Correction

The matrix element calculations predict the cross section of direct photon events with 1 to 3 parton jets, each having a minimum jet-photon mass according to a given y_{cut}. The Monte Carlo implementations of these calculations provide only the four-vectors of the photon and up to three partons. Before making a comparison, the data must be corrected to the parton level using QCD shower models. The validity of this approach for hadronic Z^0 decays with direct photons has been discussed in detail in [5, 18]. For this study the corrections are based on the JETSET [17], ARIADNE [19] and HERWIG [20] models, which simulate events with photon bremsstrahlung from quarks and give a very good description of the properties of inclusive hadronic Z^0 decays [1]. The models are used to determine bin by bin corrections for background subtracted distributions, with the bin widths chosen so as to have only small bin to bin migrations between the measured and the corrected distributions.

For an observable x, the correction $c(x)$ factorises into a contribution $c_{det}(x)$ describing the detector effects and into a contribution $c_{parton}(x)$ to correct the event to the parton level accounting for the isolation requirement and hadronisation effects

[1] The version of the QCD shower models used are JETSET 7.3, ARIADNE 4.02 and HERWIG 5.5. For JETSET and ARIADNE the parameters have been chosen according to [21]. The HERWIG model has been used with the standard parameters. The respective cut-off parameters defining the termination of the perturbative shower phase were set to 1 GeV/c^2.

$$c(x) = c_{det}(x) \cdot c_{parton}(x) = \frac{N_h(x)}{N_{det}(x)} \cdot \frac{N_p(x)}{N_h(x)}.$$

Here N_{det} denotes the number of events accepted at the detector level fulfilling the same requirements as the data. The events at the hadron level N_h have no detector simulation. They must have a photon with an energy of at least 5 GeV, fulfilling the isolation requirement, and $y_{\gamma,jet}$ has to be larger than y_{cut} for all jets. The generated events at the parton level N_p have been selected by requiring a minimum photon energy of 5 GeV and $y_{\gamma,jet} > y_{cut}$ for all jets constructed directly from the partons, but without any cone isolation requirement. Typical values are, in addition to the photon identification efficiency discussed above, 1.1 for the detector correction factors c_{det} and 1.07 for the parton correction c_{parton}.

It should be noted that in this analysis the parton correction is much smaller than in our previous publications, as the isolation angle is smaller and the cross section has not been extrapolated to photon energies below the experimental cut.

For the detector correction the generated events have been passed through a detailed simulation of the OPAL detector [22]. Possible systematic uncertainties due to imperfections in simulating the detector response and due to differences in the modelling of the photon emission will be discussed in the following subsections.

5.1 Systematic Uncertainties from the Detector Simulation

The uncertainties on the measurement of direct photon events due to possible imperfections in the detector simulation have been addressed in detail in our previous publications [4,5]. A misrepresentation of the jet energies can introduce a bias in the event selection. Assuming kinematics for massless jets, the jet energies of two jet plus photon events can be reconstructed from the photon energy and the three angles between the jets and the photon. These reconstructed jet energies E_{recon} have been compared with directly measured jet energies E_{meas}. To check how well the simulation reproduces the quality of the jet energy measurement, the shift,

$$\delta E = \frac{E_{recon} - E_{meas}}{E_{meas}}.$$

has been compared between data and events with full detector simulation using JETSET [17] as event generator. The difference of the average shifts has been found to be 0.016 ± 0.020. Similarly, a potential shift of the jet angles can be estimated, as discussed in our previous publication [5], yielding $\delta\alpha = 0.2 \pm 0.4$ degrees. Here $\delta\alpha$ is the difference between data and simulation of the determination of the jet angle. To take these effects into account, uncertainties due to shifts of 1.6% of the energy and 0.2 degrees of the jet angles were included in the systematic error for each bin.

For this analysis, event samples generated with ARIADNE [19] and HERWIG [20] as input were also available. As the detector simulation for all samples is the same the correction factors agree within their statistical errors, as expected. Therefore all three samples have been used together for the determination of the detector corrections.

5.2 Systematic Uncertainties from the Modelling of the Photon Emission

As detailed in our previous publications [4, 5] potential systematic misrepresentations of the photon emission have been investigated by studies of the particle and energy flow around the photon candidate. The parton correction splits into two parts, one accounting for the losses due to the isolation requirement and a second one for the hadronisation effects on the jet axis determination. At y_{cut} values 0.02, 0.06 and 0.2, a fraction of 7%, 6% and 10% of the events are rejected due to the isolation requirement, respectively. A systematic uncertainty of 25% has been assigned to these losses as discussed in [3]. For the hadronisation correction a systematic error of 3% has been assigned [18], which agrees with QCD studies of inclusive hadronic Z^0 decays [23]. The quadratic sum of these two uncertainties leads to a typical systematic error of 3.5 - 5%, which is assumed to be uncorrelated between the different bins and is assigned to each bin of the distributions under study.

6 The Matrix Element Calculations

Since the first measurement of final state photon radiation at LEP [2], when JETSET was the only available model, several theoretical predictions have been developed. With the addition of direct photon radiation to ARIADNE and HERWIG, all the commonly used QCD shower models now have the option of simulating quark bremsstrahlung. In the QCD shower approach the final state is obtained iteratively, using a collection of theoretically predicted parton branchings. An alternative ansatz to describe photon radiation from quarks are matrix element calculations. Recently, Monte Carlo methods to evaluate the $\mathcal{O}(\alpha\alpha_s)$ matrix element calculations have been developed by Kramer and Spiesberger [8], Glover and Stirling [9] and by Kunszt and Trocsanyi [10], yielding predictions with at most three partons and a photon in the final state.

As the matrix element calculations are of finite order perturbation theory, cuts on the phase space have to be introduced to avoid singularities in the cross section. In lowest order QED, singularities in the cross section arise from photons collinear to either the quark or the antiquark and from soft photons. In particular, the prediction of the rate of 1-jet plus photon events, in which all partons are combined into a single jet, depends on the restriction of the phase space for collinear photon emission. The selection procedure excludes the photon from the jet definition, therefore non-isolated photons are not rejected automatically. For example, if a quark radiates a collinear high energy photon, this low energy quark and the antiquark can be combined into a single jet with a jet-photon mass larger than the required y_{cut}.

In the first order in α_s additional singularities arise from soft or collinear gluon radiation, which can be treated so that they cancel against contributions from virtual gluon corrections. The limited order in $\alpha\alpha_s$ also implies that configurations with more than three jets and a photon, which occur at very low values of y_{cut}, are not predicted by the calculation.

The matrix element calculations apply two different approaches to avoid the photon-quark singularities. EEPRAD [9] of Glover and Stirling and the calculation of Kunszt and Trocsanyi

[10] use cuts on the photon energy and the quark-photon angle. GNJETS [8] has the alternative option to restrict the minimum photon-quark mass. To compare the two different approaches we compare GNJETS and EEPRAD with the data.

In EEPRAD the minimum photon energy has been set to 5 GeV, the same value as in the data. For the isolation angle 10 degrees has been chosen. This is formally the same value as for the data, however in the calculation the isolation is with respect to the partons. There is no unambiguous relation between the isolation angles with respect to particles and partons. Fragmentation effects lead to a broadening of the distribution of particles relative to the individual parton direction and it is therefore the jets which correspond more closely to the parton structure than the hadrons. In general, the cross section and event configuration depend on the value of the cut-off parameters chosen, which is discussed in detail in [18]. The dependence of the absolute cross section on the isolation angle is relatively small, because an increase of the 1-jet and 3-jet rates as a function of the isolation angle is compensated for by a decrease of the 2-jet rate.

In GNJETS the energy and isolation cuts are combined by the requirement of a minimum mass y_γ of the photon with the quark or the antiquark. The dependence of the cross section and jet rates on this cut has been studied in detail in [18]. For this calculation a compensation of changes in the 1-jet and 2-jet rates has been again observed, reducing the dependence of the absolute cross section on this variable.

As discussed in detail in [18], there is a range of y_γ values for which the prediction is rather independent of the actual value of y_γ. Firstly, the value of y_γ must be significantly lower than the lowest experimental y_{cut} value, which is 0.02 for this analysis. On the other hand it must be higher than the hadron masses, corresponding to a y_γ value of approximately 10^{-4}, to avoid non-perturbative QCD effects becoming important, since these are not included in the calculation. For this analysis the value of y_γ has been chosen to be 10^{-3}, well within the above range.

In both calculations, the singularities due to the soft and collinear gluon contributions are eliminated by integrating over a small phase space region containing the singularity and by combining the result with the virtual corrections to the direct photon cross section. These two contributions only cancel if the phase space for the gluon is not restricted, which contradicts the requirement for perfect isolation of the photon. Therefore in EEPRAD low energy gluons are allowed inside the isolation cone if the gluon-photon mass is below a small value y_0. In GNJETS quarks and gluons are not resolved and are treated as a single parton if the quark-gluon mass is below a certain value y_0, independent of any gluon photon separation. For both calculations the cross section is independent of y_0 provided its value is small relative to the y_{cut} values used.

7 Properties of Events with Final State Photons

In this section the properties of events with final state photons are compared with the predictions of the matrix element calculations. The distributions are fully corrected for backgrounds, detector effects, inefficiencies due to the photon selection, the isolation requirement and hadro-

nisation. The distributions contain all hadronic Z^0 decays with a final state photon above 5 GeV, corrected to the parton level and fulfilling $y_{\gamma,jet} > y_{cut}$.

Besides the parameters restricting the phase space, the predictions of both calculations depend on two physical parameters, the electroweak quark coupling constants and the strong coupling constant α_s. The electroweak couplings only affect the total cross section but do not influence the photon properties or the relative jet rates. Therefore this analysis, in which normalised distributions are considered, is independent of the choice of the electroweak couplings.

The discussion starts with the relative jet rates determined with the JADE E0 reconstruction scheme. In a first step only the relative 3-jet and 2-jet rates are considered which allow the strong coupling constant $\alpha_s^{(1)}$ to be determined, where the superscript indicates that this parameter is obtained from a calculation in first order QCD. The allowed range for $\alpha_s^{(1)}$ from the jet rates will be used as input parameter to the calculations, which are then compared to various event properties for three values of y_{cut} - 0.02, 0.06 and 0.2, which correspond to jet-photon masses exceeding about 13 GeV/c^2, 22 GeV/c^2 and 41 GeV/c^2, respectively. The y_{cut} values have been chosen so that the different jet multiplicities are important. As can be seen from fig. 1, for $y_{cut} = 0.02$ the 3-jet rate is still sizeable. For $y_{cut} = 0.06$ about 90% of the events are 2-jet events and for the highest value of y_{cut} most of the events are of the 1-jet plus photon type.

The size of higher order corrections can be different for different observables. To assess their size, an attempt is made to fit the value of $\alpha_s^{(1)}$ for several distributions and to use it as a parameter which might indicate the importance of higher order QCD effects. In addition to the systematic uncertainties discussed in section 5, which to a large extent affect all bins similarly, we particularly consider systematic uncertainties on $\alpha_s^{(1)}$ due to hadronisation effects and potential misrepresentations of the reconstruction of the jet energies and angles. To estimate hadronisation corrections the observables have been corrected using only ARIADNE and JETSET, or by HERWIG alone. The difference between the two results leads to uncertainties on $\alpha_s^{(1)}$ between 0.002 and 0.012. The systematic error due to the jet reconstruction was estimated from the maximum effect of smearing the jet energies by 10% or shifting them by $\pm 5\%$ and by smearing the angle between the photon and the nearest jet by 4 degrees or shifting it by ± 2 degrees. Together with the error sources discussed above, for all considered values of y_{cut} the combined systematic uncertainties to $\alpha_s^{(1)}$ is approximately equal to the statistical error.

7.1 The Relative Jet Rates

7.1.1 The Determination of $\alpha_s^{(1)}$ from Jet Rates

Since the three jet plus photon configuration is due to the emission of a gluon, the ratio

$$R_\gamma^3(y_{cut}) = \frac{\sigma_{3jet+\gamma}(y_{cut})}{\sigma_{2jet+\gamma}(y_{cut}) + \sigma_{3jet+\gamma}(y_{cut})}$$

is a measure of α_s, which may be determined from a comparison with the matrix element predictions. One should note that the result is obtained from a calculation to first order in $\alpha_s^{(1)}$ and has therefore no explicit dependence on the renormalisation scale. Here we use y_{cut}

		GNJETS	EEPRAD
y_{cut}	R^3_γ	$\alpha_s^{(1)}$	$\alpha_s^{(1)}$
0.02	$0.285 \pm 0.011 \pm 0.013$	$0.164 \pm 0.008 \pm 0.006$	$0.164 \pm 0.008 \pm 0.006$
0.04	$0.104 \pm 0.008 \pm 0.015$	$0.194 \pm 0.017 \pm 0.027$	$0.195 \pm 0.016 \pm 0.027$
0.06	$0.042 \pm 0.006 \pm 0.007$	$0.223 \pm 0.035 \pm 0.036$	$0.226 \pm 0.035 \pm 0.035$
0.08	$0.016 \pm 0.004 \pm 0.003$	$0.263 \pm 0.077 \pm 0.057$	$0.272 \pm 0.082 \pm 0.060$

Table 1: Measurement of the three jet fraction R^3_γ and first order α_s values for different values of y_{cut} as required by GNJETS and EEPRAD to reproduce R^3_γ. The first error is statistical, the second systematic.

values between 0.02 and 0.08. This choice is a compromise between reasonable statistics of the 3-jet plus photon rate and a low rate of 4-jet plus photon events, which are not included in the matrix element calculations.

The measured values of R^3_γ are shown in table 1, in which the first errors are statistical and the second systematic. The values of $\alpha_s^{(1)}$ that must be input to both calculations in order for them to predict a value of R^3_γ consistent with the data are also given in table 1. The $\alpha_s^{(1)}$ values required by the two calculations are in very good agreement. The $\alpha_s^{(1)}$ values for the various values of y_{cut} are compatible with each other, however, there is a trend towards an increase of $\alpha_s^{(1)}$ with y_{cut}. One should note that the jet ratios and thus the values obtained for $\alpha_s^{(1)}$ are correlated for the different y_{cut} values. The first order value of $\alpha_s^{(1)}$ of 0.177 derived from the jet rates of the inclusive sample of hadronic Z^0 decays [24] is consistent with the values obtained in this analysis. For the discussion of the relative jet rates in the following section we allow $\alpha_s^{(1)}$ to vary by 0.03 around 0.18 to show the $\alpha_s^{(1)}$ dependence as a function of y_{cut}. For the subsequent comparison of the photon properties $\alpha_s^{(1)}$ has been fixed to 0.18.

7.1.2 Comparison of the Jet Rates with Matrix Element Calculations

In fig. 1 the relative jet rates are plotted for $0.02 < y_{cut} < 0.2$ together with the predictions from GNJETS and EEPRAD. The lower bound was chosen to avoid large effects from the quark photon singularity which leads, for example, to negative 2-jet rates at y_{cut}=0.005 if high values of α_s within the considered range are chosen. The upper bound was chosen to exclude regions where this singularity becomes very important for the 1-jet plus photon rate. In interpreting the plots it is important to note that the rates at the different values of y_{cut} are correlated.

The 1-jet rate increases steadily over the entire y_{cut} range, contributing only $(0.5 \pm 0.4)\%$ at $y_{cut} = 0.02$ and reaching $(74.3 \pm 3.1)\%$ at $y_{cut} = 0.2$. As previously discussed, the 1-jet rate is the one most sensitive to the treatment of quark-photon singularities. Using the $\alpha_s^{(1)}$ range from 0.15 to 0.21, GNJETS reproduces the data well for most y_{cut} values. Only at the highest y_{cut} values does it slightly underestimate the 1-jet rate. Note that the phase space for 1-jet events increases with y_{cut}, rendering it more probable that a very high energy photon is close to a low energy quark. EEPRAD underestimates the 1-jet rate for all y_{cut} values above 0.1. This may be remedied by decreasing $\alpha_s^{(1)}$, but results in a significant disagreement in the relative

3-jet rate at smaller y_{cut}. In addition, the agreement in the 2-jet rate for y_{cut} values below 0.06 deteriorates quickly with decreasing $\alpha_s^{(1)}$.

The 2-jet rate increases from $(70.1 \pm 2.0)\%$ at $y_{cut} = 0.02$ to its maximum of $(91.8 \pm 1.4)\%$ at $y_{cut} = 0.06$ and then decreases slowly to $(25.7 \pm 3.1)\%$ at the highest considered y_{cut} value of 0.2. GNJETS describes the data well, whereas EEPRAD overestimates the relative 2-jet rate for y_{cut} values above 0.06. This observation is correlated with the disagreement in the 1-jet rate discussed in the previous paragraph. As described in [18] the *absolute* two and three jet cross sections agree very well for both $\mathcal{O}(\alpha\alpha_s)$ calculations, whereas EEPRAD predicts a significantly lower 1-jet rate. For the 1-jet rate and the 2-jet rate at y_{cut} values above 0.1, the α_s dependence of EEPRAD is larger than GNJETS.

The relative 3-jet rate decreases with increasing y_{cut}, starting from $(29.5 \pm 1.9)\%$ at the lowest considered y_{cut} value to less than 1% at $y_{cut} = 0.1$. As the calculations are only to lowest order in α_s they cannot predict events with more than three jets. At $y_{cut} = 0.02$, the data contain $(1.5 \pm 0.3)\%$ events with more than three jets, which have been added to the 3-jet events for comparison with the calculations. For higher y_{cut} values, the number of 4-jet events is negligible. Both calculations predict almost exactly the same *absolute* 3-jet cross section, with a very similar α_s dependence [18]. As can be seen from fig. 1 the observed 3-jet rates tend to favour larger $\alpha_s^{(1)}$ values with increasing y_{cut}. This is also reflected in the increase of the central value for $\alpha_s^{(1)}$ as function of y_{cut} as listed in table 1.

In general it seems that GNJETS can reasonably reproduce the jet rates within the considered $\alpha_s^{(1)}$ range. This is not the case for EEPRAD which underestimates the 1-jet rate at large values of y_{cut} when the value of $\alpha_s^{(1)}$ derived at low values of y_{cut} is used. As discussed in [25] a remedy could be the introduction of a photon fragmentation contribution. Alternatively one could also adjust the $\alpha_s^{(1)}$ value of EEPRAD or the isolation angle for each value of y_{cut}. A decrease of $\alpha_s^{(1)}$ has a similar effect to an increase of the isolation angle. Note that in this analysis the isolation angle in EEPRAD bears almost no relation to the selection criteria for the data (see for example discussion in [18]).

7.2 The Photon Properties

In this section several distributions describing the photon emission are discussed. All distributions are normalised to unity and are compared to the predictions of GNJETS and EEPRAD. The value of $\alpha_s^{(1)}$ for both calculations has been fixed to 0.18, as discussed in section 6.2. As higher order corrections can affect different observables differently, the value of α_s leading to the best agreement can vary between the different distributions. As discussed in [18], the predictions of the cross section from both matrix element calculations are very similar, with the exception of the 1-jet plus photon events, which show a larger $\alpha_s^{(1)}$ dependence in EEPRAD. For this reason the effect of varying $\alpha_s^{(1)}$ will be discussed only for EEPRAD.

	y_{cut}		
Distribution	0.02	0.06	0.20
Photon Energy	$0.045 \pm 0.026 \pm 0.025$	$0.150 \pm 0.015 \pm 0.010$	$0.158 \pm 0.013 \pm 0.015$
$E_\gamma < 40$ GeV	$0.099 \pm 0.024 \pm 0.030$	no change	no change
p_T w.r.t. thrust	-	$0.193 \pm 0.054 \pm 0.093$	-
Angle to nearest jet	$0.137 \pm 0.013 \pm 0.010$	$0.155 \pm 0.020 \pm 0.020$	-

Table 2: First order α_s values leading to the best description of the data by EEPRAD. The first error is statistical, the second systematic. Missing entries are due to failures of the χ^2 test.

7.2.1 The Photon Energy Spectrum

Both matrix element predictions can reproduce the overall shape of the photon energy spectrum for all three y_{cut} values (fig. 2). For y_{cut}=0.02 the spectrum predicted by both calculations is somewhat harder than the measured one. At the two higher y_{cut} values EEPRAD predicts a lower rate of photons above 42 GeV than GNJETS. This is the kinematic region sensitive to the phase space cuts discussed above, for which a photon of almost beam energy can be very close to a low energy quark.

For EEPRAD the energy spectrum has been created for nine different values of $\alpha_s^{(1)}$ between 0 and 0.25. For each value of $\alpha_s^{(1)}$ a χ^2 test has been performed to determine the level of agreement between the measured photon spectrum and the prediction from EEPRAD. As the systematic errors from the correction procedure are significant, they have been included in the χ^2 calculation. The $\alpha_s^{(1)}$ leading to the best description has been determined from the minimum of a second order polynomial, defined by the three lowest χ^2 values. In figs. 3a to 3d the χ^2 distributions are shown for the different y_{cut} values. To estimate the systematic uncertainty of $\alpha_s^{(1)}$ due to the correction procedure the same checks have been performed as for the jet rate ratio R_γ^3 described in section 7.1.1. The results are listed in table 2. For $y_{cut} = 0.02$ a minimal χ^2 of 20.0 for 16 bins has been found for a value of $\alpha_s^{(1)} = 0.045 \pm 0.026 \pm 0.025$, with which the low energy region of the photon spectrum is well described, although the number of photons with more than 40 GeV is still overestimated. This value of α_s is significantly lower than the 0.164 ± 0.010 obtained from the jet rates for this value of y_{cut}, which may indicate the importance of higher order corrections.

At y_{cut}=0.06 a minimum χ^2 of 9.4 for 16 bins is found for $\alpha_s^{(1)} = 0.150 \pm 0.015 \pm 0.010$. This value is about two standard deviations lower than that obtained from the jet rates. By reducing $\alpha_s^{(1)}$, the agreement slowly improves for low energies, but the relative 1-jet rate is quickly enhanced leading to a strong increase in the rate of photons with almost beam energy, which is the dominant contribution to the χ^2 for $\alpha_s^{(1)}$ values below 0.15.

At y_{cut}=0.2 the spectrum is dominated by 1-jet plus photon events and the enhancement of the high energy part of the spectrum with decreasing α_s is even stronger. Here an α_s value of $0.158 \pm 0.013 \pm 0.015$ gives a minimum χ^2 of 3.1 for 11 bins, which is consistent with the value of 0.18 ± 0.03 used for the comparison.

If one excludes photons above 40 GeV from the χ^2 calculation at y_{cut}= 0.02 the best description is found for $\alpha_s^{(1)} = 0.099 \pm 0.024 \pm 0.030$, resulting in a χ^2 of 4.0 for 14 bins (fig. 3b). The sensitivity of α_s further suggests that higher order corrections are important in QCD for this y_{cut} value. For the other y_{cut} values no significant shift of the $\alpha_s^{(1)}$ is found, if the highest energy photons are excluded. Also shown in fig. 2 is the prediction of JETSET, which includes some higher order QCD effects. It describes the data well for all values of y_{cut}, indicating that the addition of higher order QCD effects can improve the agreement between data and the calculations.

7.2.2 The Transverse Momentum with respect to the Thrust Axis

In fig. 4 the transverse momentum of the photon with respect to thrust axis is plotted. The thrust has been calculated from all tracks and clusters including the photon candidate. The transverse momentum is kinematically limited to $1/\sqrt{3}\,E_{beam} \approx 27$ GeV/c. Transverse momentum close to zero is due to high energy photons that define the thrust axis. A fraction of these events are of the 1-jet plus photon configuration. According to JETSET they amount to (8.1 $\pm$ 1.8)%, (36.2 $\pm$ 3.1)% and (81.2 $\pm$ 2.4)% of the events with a transverse momentum below 2.5 GeV for the three y_{cut} values 0.02, 0.06 and 0.2, respectively. For the two lower y_{cut} values both matrix element calculations describe the shape of the distributions well, whereas for $y_{cut} = 0.2$, both calculations underestimate the number of events with very low transverse momentum. Again, this is related to the deficiencies in reproducing the 1-jet plus photon rate at the high y_{cut}. Below 15 GeV/c the data fall off more quickly than the predictions.

For EEPRAD this distribution has been generated with various $\alpha_s^{(1)}$ values. Using the same procedure as for the energy spectrum the $\alpha_s^{(1)}$ value with the lowest χ^2 has been determined. In general, the dependence of the χ^2 value on $\alpha_s^{(1)}$ is smaller than for the energy spectrum. For the y_{cut} values of 0.02 and 0.2 the test fails as the χ^2 distribution has no local minimum, the smallest χ^2 being obtained for $\alpha_s^{(1)}$ about zero. For $y_{cut} = 0.06$, a minimum χ^2 of 25.3 for 10 bins has been found for $\alpha_s^{(1)} = 0.193 \pm 0.05 \pm 0.09$, which is in agreement with the value derived from the jet rates. The results of varying $\alpha_s^{(1)}$ for the different distributions are summarised in table 2.

7.2.3 The Transverse Momentum with respect to the Jet Direction

The transverse momentum of the photon with respect to the jet with the lowest jet-photon mass, may be interpreted in the context of QCD shower models as a measure of the time evolution of the emission process. A small transverse momentum is in general the result of a later emission with the chance of gluon emission before the photon emission. Comparing this observable with a prediction from a matrix element calculation, particularly at low p_T might indicate to what extent higher order terms in the calculation influence the event topology.

The transverse momentum is shown in fig. 5. Due to the minimum photon momentum of 5 GeV/c the spectra have a sharp edge around 5 GeV/c. Events with almost zero transverse momentum are 1-jet plus photon events. EEPRAD underestimates their number for $y_{cut} = 0.06$ and 0.2. At $y_{cut} = 0.02$ and $y_{cut} = 0.06$ EEPRAD and GNJETS overestimate the number of

photons with more than 40 GeV/c transverse momentum. This is partly due to the somewhat harder energy spectrum of the predictions. In addition, it is related to rare events with a very low energy jet approximately perpendicular to a photon of almost beam energy. It might be expected that these events are particularly sensitive to additional gluon radiation.

At $y_{cut} = 0.2$ both calculations predict more 2-jet plus photon events with transverse momentum between 18 GeV/c and 35 GeV/c than observed in the data. Part of this effect is related to the normalisation and the underestimation of the 1-jet plus photon rate. A significant disagreement is observed for 2-jet events with a transverse momentum of 20-25 GeV/c. Lowering α_s increases the 1-jet rate, resulting in an increase at zero transverse momentum, but it does not remedy the disagreement in the 20-25 GeV/c region.

7.2.4 The Angle with respect to the Jet

The angle with respect to the jet with the lowest jet-photon mass is shown in fig. 6. This angle is correlated with the transverse momentum discussed in the previous section. The selection criteria for photons exclude events below 30, 45 and 90 degrees for the three y_{cut} values 0.02, 0.06 and 0.2, respectively. The 1-jet plus photon events show up in this plot at 180 degrees. At y_{cut}=0.02 the data show a broad peak around 70 degrees, whilst both calculations tend to have most events around 50 degrees. The measurements for the higher y_{cut} values are well described by both calculations, except for a disagreement between data and EEPRAD for jet-photon angles above 165 degrees correlated with the underestimation of the 1-jet plus photon rate by EEPRAD.

For the y_{cut} values 0.02 and 0.06, the $\alpha_s^{(1)}$ value giving the lowest χ^2 has again been determined. At $y_{cut} = 0.02$ the data are best described with $\alpha_s^{(1)} = 0.137 \pm 0.013 \pm 0.010$ which is about two standard deviations below the value obtained from the jet rates. At $y_{cut} = 0.06$, $\alpha_s^{(1)}$ has been determined to be $0.155 \pm 0.020 \pm 0.020$, consistent with the number from the jet rates.

7.2.5 The Jet-Photon Mass

The minimum mass of the photon and any jet of the event is shown in fig. 7. The kinematic limit for 2-jet plus photon events is around 60 GeV and the 1-jet plus photon events appear at the centre-of-mass energy. Both calculations describe the shape of the distributions. The underestimation of the 1-jet plus photon rate by EEPRAD at the two higher y_{cut} values can be seen clearly.

8 Summary

Properties of hadronic Z^0 decays with final state photons have been compared with the predictions of two $\mathcal{O}(\alpha\alpha_s)$ matrix element calculations, EEPRAD [9] and GNJETS [8], which are implemented by a Monte Carlo method. The two approaches differ in the definition of phase

space boundaries for photon and gluon emission. Neither of them includes the quark-to-photon fragmentation function which is a theoretically well founded way to treat the quark-photon singularities in the calculations. Note that this function has to be determined from data. For this comparison the experimental distributions have been corrected to the parton level taking into account effects from the experimental photon isolation, background, detector and hadronisation.

As a first step, the values of $\alpha_s^{(1)}$ for the first order calculations have been determined from the ratio of 3-jet events to the sum of 2-jet and 3-jet events for various values of y_{cut} in the range $0.02 \leq y_{cut} \leq 0.08$. Both calculations need the same values of $\alpha_s^{(1)}$ to describe the data. The jet multiplicity ratio can be consistently described with $\alpha_s^{(1)} = 0.18 \pm 0.03$, which is used as the input $\alpha_s^{(1)}$ value for comparison of other event properties.

With this range of values for $\alpha_s^{(1)}$, GNJETS describes the relative jet rates over the full range of the considered y_{cut} values. For $y_{cut} \geq 0.1$ EEPRAD underestimates the relative 1-jet rate and correspondingly overestimates the relative 2-jet rate. Previous studies indicate that this deviation is due to the underestimate of the absolute production of 1-jet events by EEPRAD [18].

Further properties of events with photons have been compared with the matrix element predictions for the y_{cut} values 0.02, 0.06 and 0.2. At $y_{cut} = 0.02$ both calculations describe the general shape of all the distributions investigated. However, as studied with EEPRAD, the distribution of the photon energy favours a significantly lower value of $\alpha_s^{(1)}$, indicating that higher order corrections may be important for this value of y_{cut}. This is supported by the still appreciable rate of events with more than 3 jets. At $y_{cut} = 0.06$, which corresponds to a jet-photon mass of exceeding about 22 GeV/c^2, more than 90% are 2-jet plus photon events, most of which are far away from any phase space boundary used in the calculations. At this value of y_{cut} the data agree well with the predictions from both calculations for all considered distributions, indicating that neither higher order corrections nor the details of the phase space restrictions are important to describe these events. At $y_{cut} = 0.20$ the events are mostly 1-jet events, which are most sensitive to the implementation of the phase space boundaries. Both calculations, but particularly EEPRAD, show deviations in those parts of the distributions which are related to the 1-jet plus photon configuration. If one restricts the comparison to the 2-jet plus photon topologies the distributions are well reproduced by both calculations.

In general, we observe that GNJETS can describe the data reasonably with $\alpha_s^{(1)} = 0.18$. For EEPRAD a χ^2 test has been performed for the spectra of the photon energy, its momentum transverse to the thrust direction and its angle to the closest jet direction to find the $\alpha_s^{(1)}$ value giving the best description of the data. For $y_{cut} = 0.02$, values of $\alpha_s^{(1)}$ varying between 0.045 and 0.137 lead to the best description of the data for different distributions. This variation of $\alpha_s^{(1)}$ is interpreted as an indication of the need for higher order corrections. At $y_{cut} = 0.06$ all distributions can be described with $\alpha_s^{(1)}$ values consistent with those derived from the jet rates.

The good description of the data for y_{cut} values around 0.06 by both calculations, especially for photons below 40 GeV, the small dependence of the predictions on $\alpha_s^{(1)}$, together with the previously found agreement between the calculations for the predicted absolute 2-jet plus photon and 3-jet plus photon cross section [18] make them suitable in this kinematical region for measurements requiring a reliable prediction of the *absolute* photon cross section, such as

the determination of the electroweak coupling constants [26].

9 Acknowledgements

We thank N. Glover and H. Spiesberger for many interesting discussions.

It is a pleasure to thank the SL Division for the efficient operation of the LEP accelerator, the precise information on the absolute energy, and their continuing close cooperation with our experimental group. In addition to the support staff at our own institutions we are pleased to acknowledge the

Department of Energy, USA,
National Science Foundation, USA,
Particle Physics and Astronomy Research Council, UK,
Natural Sciences and Engineering Research Council, Canada,
Fussefeld Foundation,
Israel Ministry of Science,
Israel Science Foundation, administered by the Israel Academy of Science and Humanities,
Minerva Gesellschaft,
Japanese Ministry of Education, Science and Culture (the Monbusho) and a grant under the Monbusho International Science Research Program,
German Israeli Bi-national Science Foundation (GIF),
Direction des Sciences de la Matière du Commissariat à l'Energie Atomique, France,
Bundesministerium für Forschung und Technologie, Germany,
National Research Council of Canada,
A.P. Sloan Foundation and
Junta Nacional de Investigação Científica e Tecnológica, Portugal.

References

[1] T.F.Walsh and P.Zerwas, Phys.Lett. B44 (1973), 195; S.J.Brodsky, C.E.Carlson, and R.Suaya, Phys.Rev. D14 (1976), 2264; K.Koller, T.F.Walsh, and P.Zerwas, Z.Phys. C2 (1979), 197; E.Laermann, T.F.Walsh, I.Schmitt, and P.M.Zerwas, Nucl.Phys. B207 (1982), 205.

[2] OPAL Collaboration, M.Z.Akrawy et al., Phys. Lett. B246 (1990), 285.

[3] OPAL Collaboration, G. Alexander et al., Phys. Lett. B264 (1991), 219.

[4] OPAL Collaboration, P. D. Acton et al., Z.Phys. C54 (1992), 193.

[5] OPAL Collaboration, P. D. Acton et al., Z. Phys. C58 (1993), 405.

[6] ALEPH Collaboration, D. Decamp et al., Phys.Lett. B264 (1991), 476; DELPHI Collaboration, P. Abreu et al., Z.Phys. C53 (1992), 555; L3 Collaboration, O.Adriani et al., Phys. Lett. B292 (1992), 472; L3 Collaboration, O.Adriani et al., Phys. Lett. B301 (1993), 136; ALEPH Collaboration, D. Decamp et al., Phys. Lett. B264 (1991), 476; ALEPH Collaboration, D. Buskulic et al., Z. Phys. C57 (1993), 17.

[7] G. Kramer, B. Lampe, Phys. Lett. B269 (1991), 401.

[8] G. Kramer and H. Spiesberger, in the Proceedings of the Workshop on Photon Radiation from Quarks, Annecy, Dec 2-3 1991, ed. S.Cartwright, CERN 92-04; DESY 92-022.- In these references the GNJETS calculation is described.

[9] E. W. N. Glover and J. Stirling, Phys. Lett. B295 (1992), 128. - In this reference the EEPRAD calculation is described.

[10] Z. Kunszt and Z. Trocsanyi, Nucl. Phys. B394 (1993), 139.

[11] OPAL Collaboration, K. Ahmet et al., Nucl. Instr. Meth. A305 (1991), 275.

[12] OPAL Collaboration, G. Alexander et al., Z. Phys. C52 (1991), 175.

[13] JADE Collaboration, W. Bartel et al., Z. Phys. C33 (1986), 23; JADE Collaboration, S. Bethke et al., Phys. Lett. B123 (1988), 235.

[14] OPAL Collaboration, M. Z. Akrawy et al., Phys. Lett. B253 (1991), 511.

[15] OPAL Collaboration, R. Akers et al., Z. Phys. C63 (1994), 181.

[16] F. A. Berends, R. Kleiss, S. Jadach, Nucl. Phys. B202 (1982), 63.

[17] T. Sjöstrand, Comp. Phys. Comm. 39 (1986), 347; JETSET, Version 7.2.

[18] P. Mättig, H. Spiesberger, W. Zeuner, Z. Phys. C60 (1993), 613.

[19] U. Petterson, LU TP 88-5 (1988); U. Petterson, L. Lönnblad, LU TP 88-15 (1988); L. Lönnblad LU TP 89-10 (1989); L. Lönnblad, in Proceedings of the Workshop on Photon Radiation from Quarks, Annecy Dec, 2-3 1991, ed. S.Cartwright, CERN 92-04.

[20] G. Marchesini and B. R. Webber, Nucl. Phys. B238 (1984), 1; B. R. Webber, Nucl. Phys. B238 (1984), 492; G. Abbiendi et al., Comp.Phys.Comm. 67 (1992), 465; M. H. Seymour, in Proceedings of the Workshop on Photon Radiation from Quarks, Annecy Dec, 2-3 1991, ed. S.Cartwright, CERN 92-04, Z. Phys. C56 (1992), 161.

[21] OPAL Collaboration, M. Z. Akrawy et al., Z. Phys. C47 (1990), 505.

[22] J. Allison et al., Nucl.Instr.Meth. A317 (1992), 47; R. Brun et al., GEANT3 User's Guide, CERN DD/EE/84-1 (1989).

[23] OPAL Collaboration, P. D. Acton et al., Z. Phys. C55 (1992), 1.

[24] For the determination of $\alpha_s^{(1)}$ the jet rates of Phys.Lett. B235 (1990) 389 were fitted with a first order QCD calculation.

[25] E. W. N. Glover, A. G. Morgan, Z.Phys C62 (1994) 311.

[26] P. Mättig, W. Zeuner, Z.Phys. C52 (1991), 31.

Figure Caption

Fig. 1 Relative jet rates compared to EEPRAD (a) and GNJETS (b). The points are the measurement, the lines are predictions.

Fig. 2 Photon energy spectrum for three values of y_{cut} (0.02, 0.06 and 0.2). The data are shown as full points and the predictions as histograms. Both matrix element calculations are shown for $\alpha_s^{(1)}$=0.18. The isolation angle in EEPRAD is 10 degrees. The dashed histogram shows the predictions of JETSET.

Fig. 3 The χ^2 values from the comparison of the photon energy spectrum with the predictions from EEPRAD for different values of α_s. The curve is the second order polynomial defined by the three lowest values of χ^2. Fig 3a and b show the comparison for $y_{cut} = 0.02$, where in (a) the full energy range is considered, in (b) only photon energies < 40 GeV, 3c for $y_{cut} = 0.06$ and 3d for $y_{cut} = 0.2$.

Fig. 4 Transverse momentum of the photon with respect to the thrust axis for three values of y_{cut} (0.02, 0.06 and 0.2). The data are shown as full points and the predictions as histograms. Both calculations are shown for $\alpha_s^{(1)}$=0.18. The isolation angle in EEPRAD is 10 degrees.

Fig. 5 Transverse momentum of the photon with respect to the jet with the minimum jet photon mass for three values of y_{cut} (0.02, 0.06 and 0.2). The data are shown as full points and the predictions as histograms. Both calculations are shown for $\alpha_s^{(1)}$=0.18. The isolation angle in EEPRAD is 10 degrees.

Fig. 6 The angle of the photon with respect to the jet with the minimum jet-photon mass for three values of y_{cut} (0.02, 0.06 and 0.2). The data are shown as full points and the predictions as histograms. Both calculations are shown for $\alpha_s^{(1)}$=0.18. The isolation angle in EEPRAD is 10 degrees.

Fig. 7 The minimum jet-photon mass for three values of y_{cut} (0.02, 0.06 and 0.2). The data are shown as full points and the predictions as histograms. Both calculations are shown for $\alpha_s^{(1)}$=0.18. The isolation angle in EEPRAD is 10 degrees.

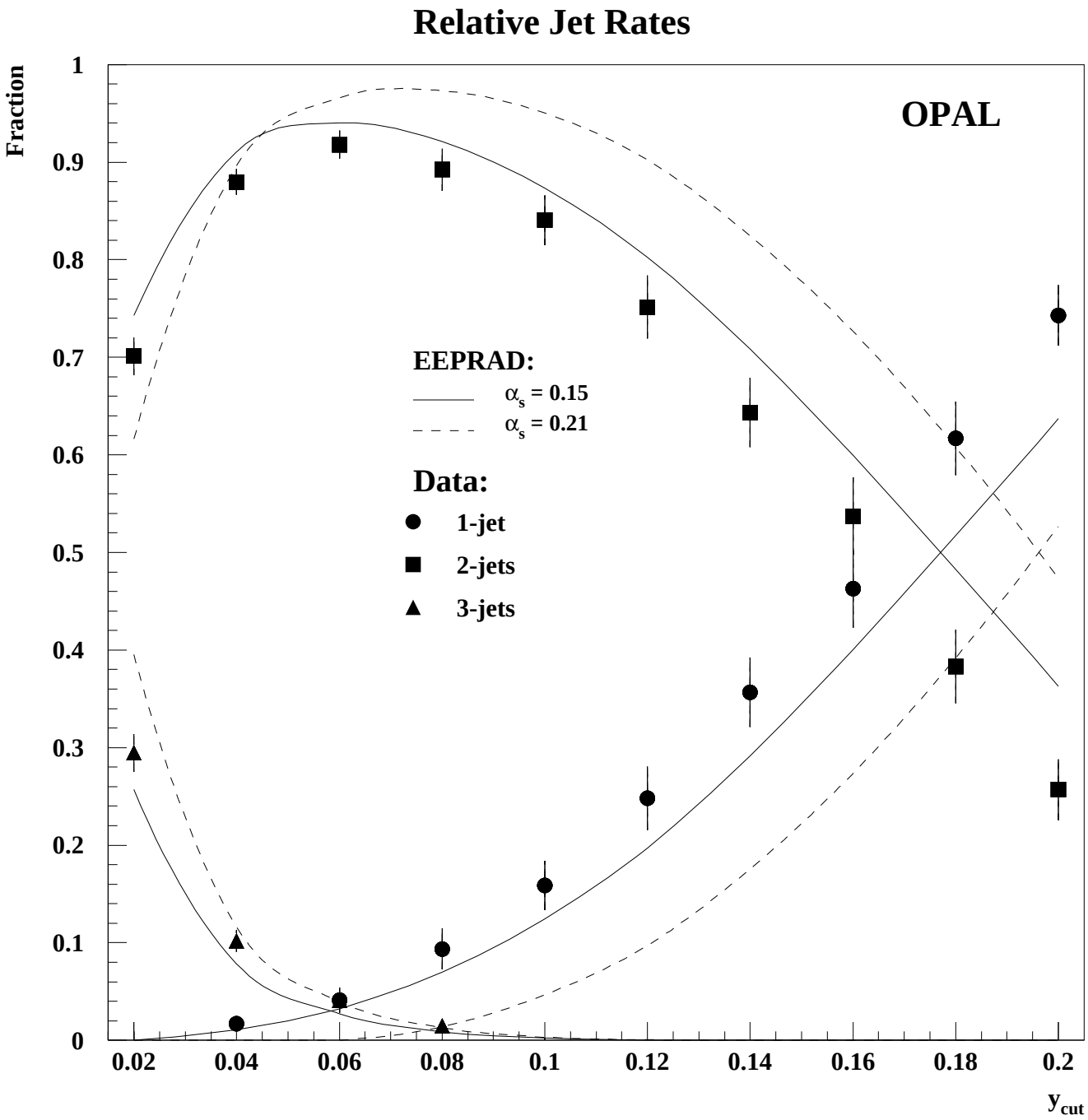
Relative Jet Rates
OPAL
Fraction
1
0.9
0.8
0.7
0.6
0.5
0.4
0.3
0.2
0.1
0
EEPRAD:
α_s = 0.15
α_s = 0.21
Data:
1-jet
2-jets
3-jets
0.02
0.04
0.06
0.08
0.1
0.12
0.14
0.16
0.18
0.2
y_{cut}

Figure 1a

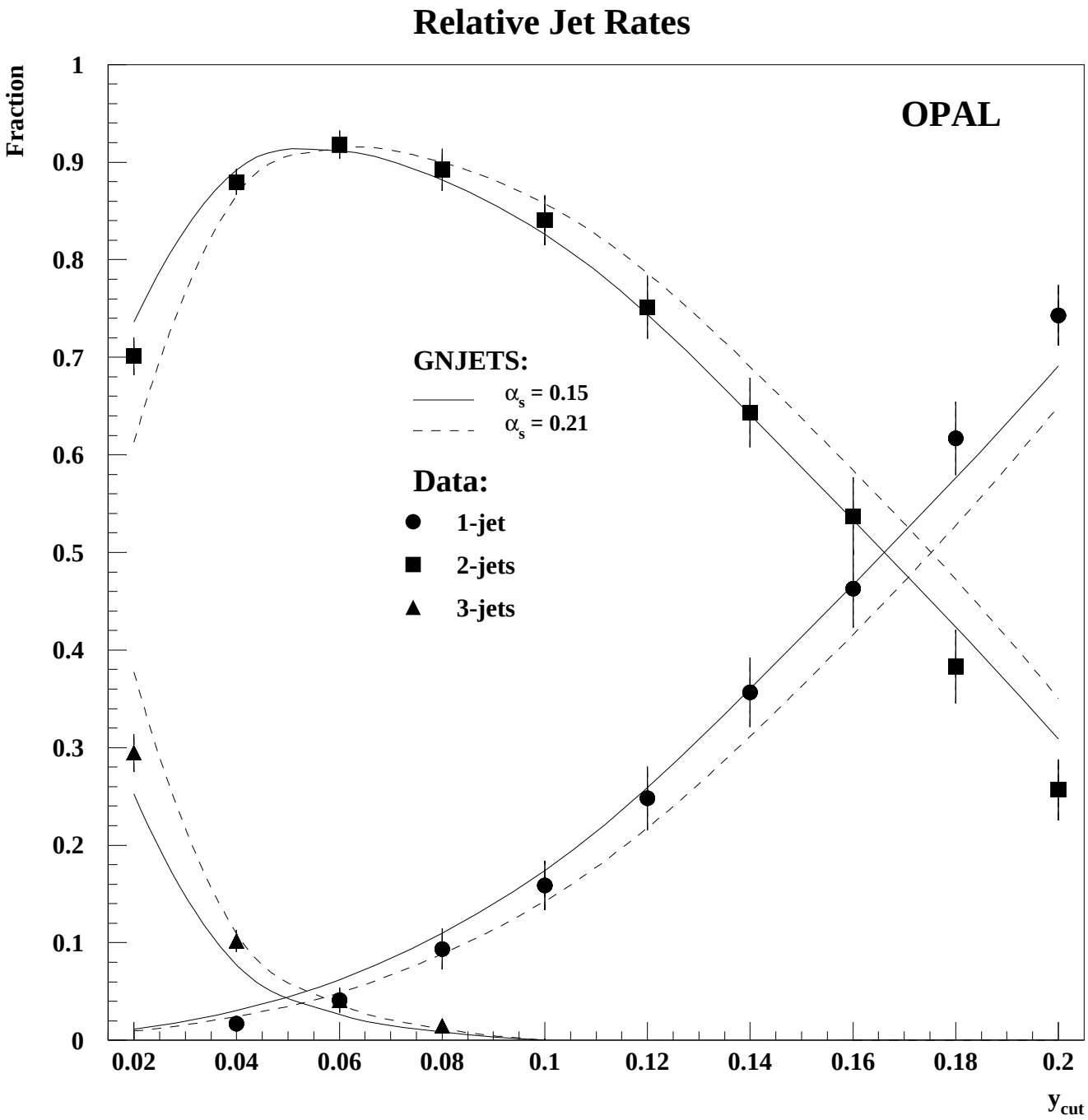
Relative Jet Rates
OPAL
Fraction
1
0.9
0.8
0.7
0.6
0.5
0.4
0.3
0.2
0.1
0
GNJETS:
α_s = 0.15
α_s = 0.21
Data:
1-jet
2-jets
3-jets
0.02
0.04
0.06
0.08
0.1
0.12
0.14
0.16
0.18
0.2
y_{cut}

Figure 1b

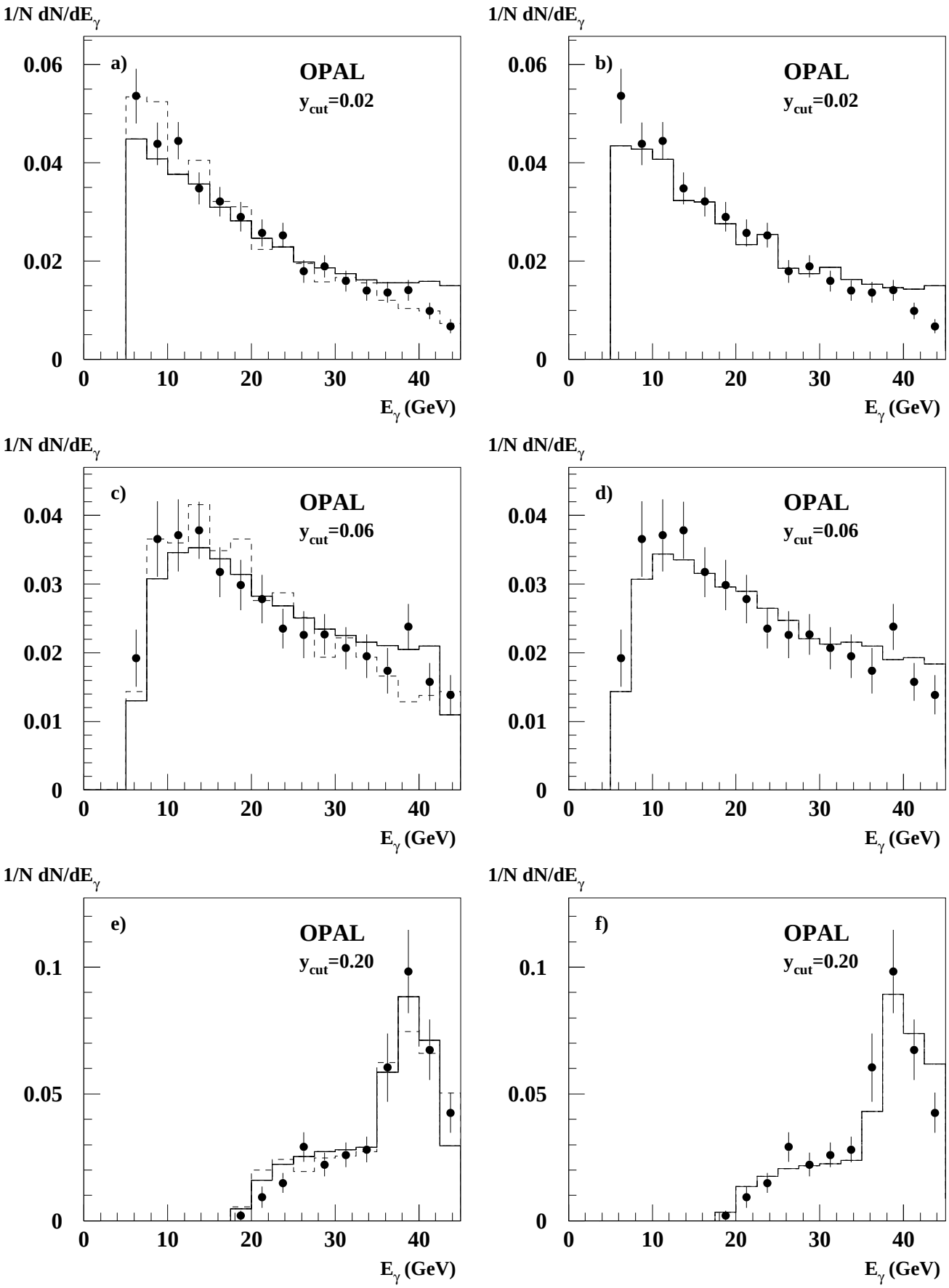
EEPRAD
GNJETS
1/N dN/dE$_\gamma$
a)
b)
c)
d)
e)
f)
OPAL
y_{cut}=0.02
y_{cut}=0.06
y_{cut}=0.20
E$_\gamma$ (GeV)

Figure 2

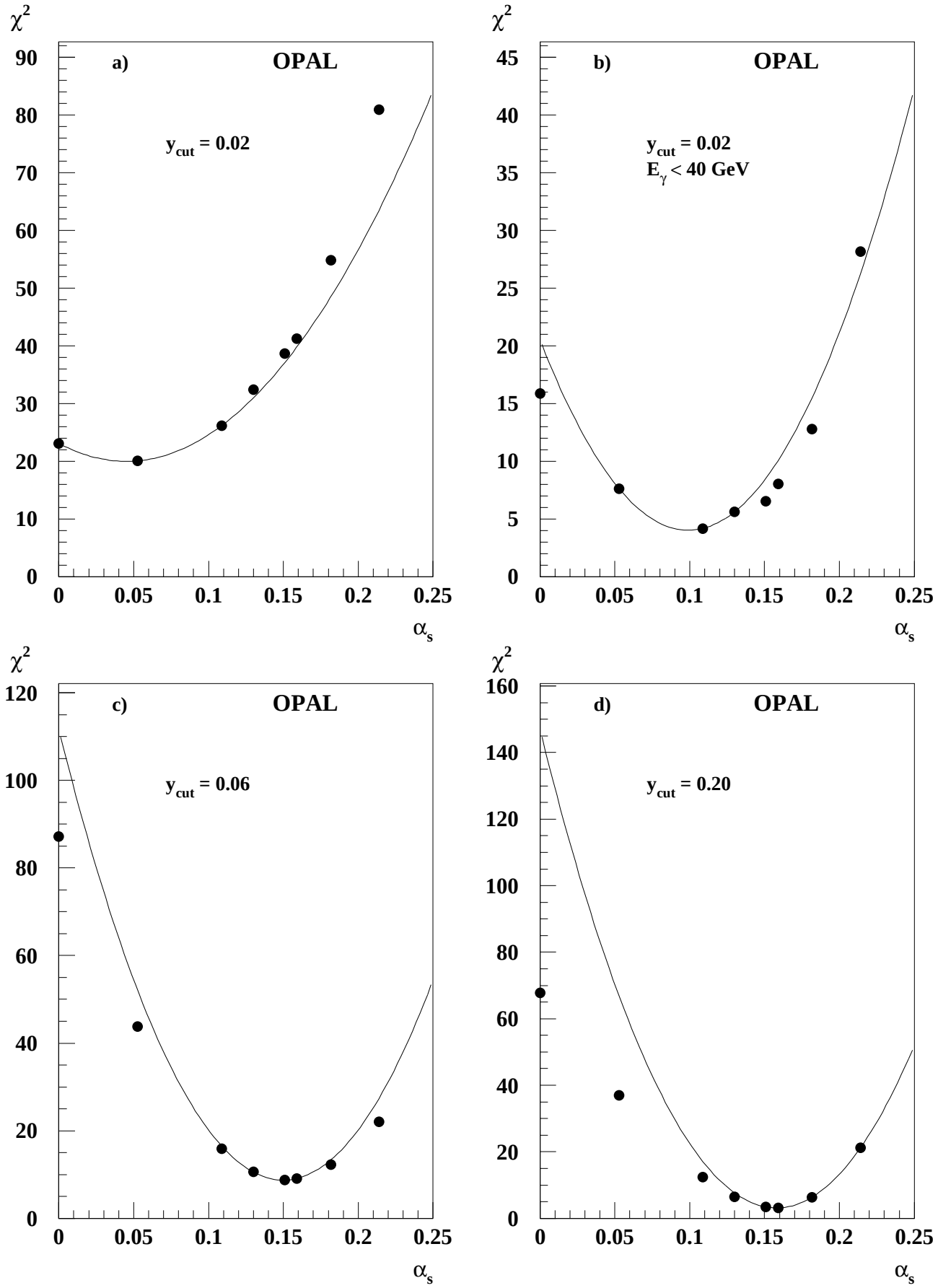
a)
OPAL
y_{cut} = 0.02
b)
OPAL
y_{cut} = 0.02
E_γ < 40 GeV
c)
OPAL
y_{cut} = 0.06
d)
OPAL
y_{cut} = 0.20
χ^2
α_s

Figure 3

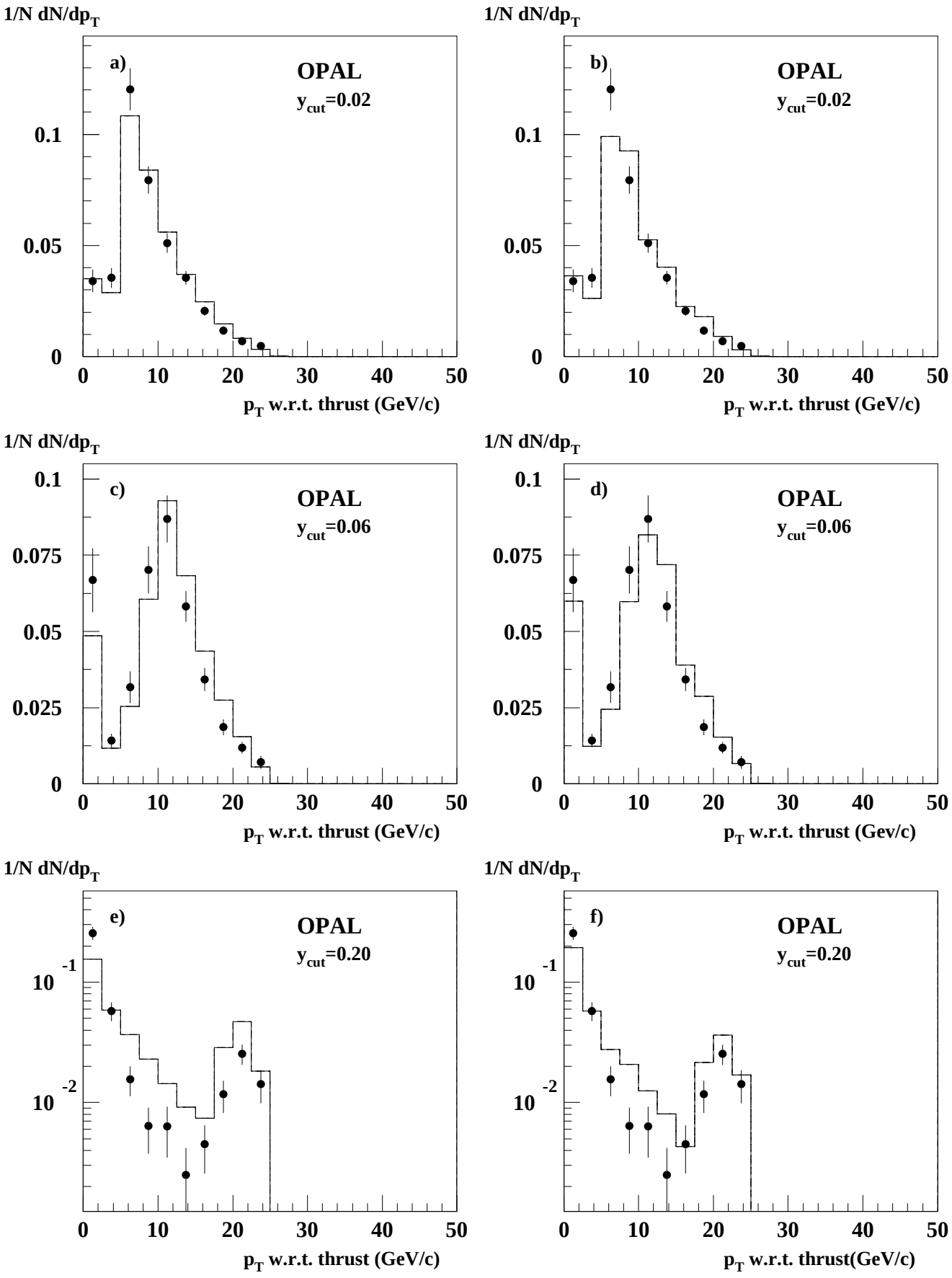
EEPRAD
GNJETS
1/N dN/dp$_T$
a)
OPAL
y$_{cut}$=0.02
b)
OPAL
y$_{cut}$=0.02
c)
OPAL
y$_{cut}$=0.06
d)
OPAL
y$_{cut}$=0.06
e)
OPAL
y$_{cut}$=0.20
f)
OPAL
y$_{cut}$=0.20
p$_T$ w.r.t. thrust (GeV/c)
p$_T$ w.r.t. thrust (Gev/c)
p$_T$ w.r.t. thrust(GeV/c)

Figure 4

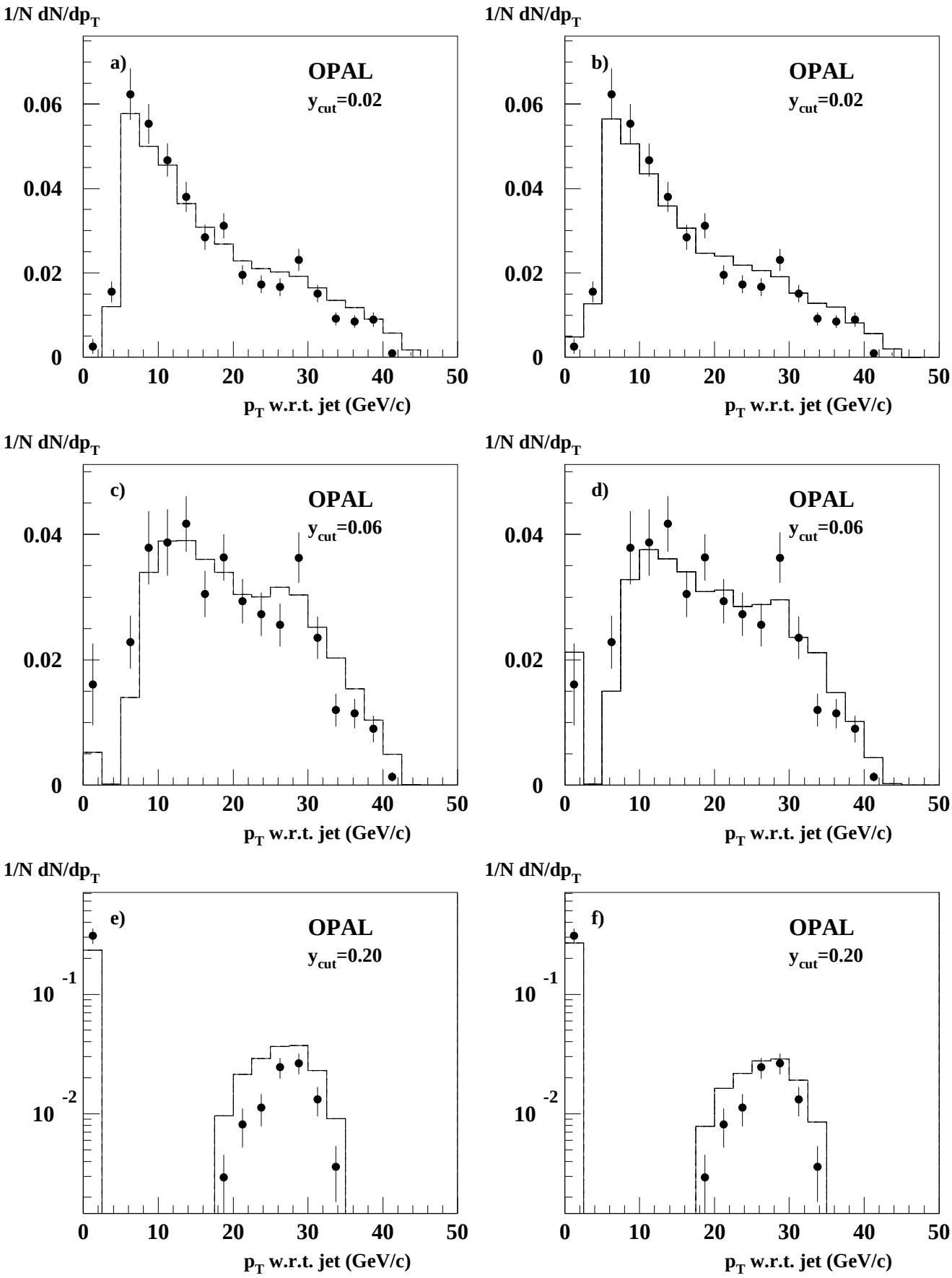
EEPRAD
GNJETS
1/N dN/dp_T
a)
OPAL
y_cut=0.02
b)
OPAL
y_cut=0.02
c)
OPAL
y_cut=0.06
d)
OPAL
y_cut=0.06
e)
OPAL
y_cut=0.20
f)
OPAL
y_cut=0.20
p_T w.r.t. jet (GeV/c)

Figure 5

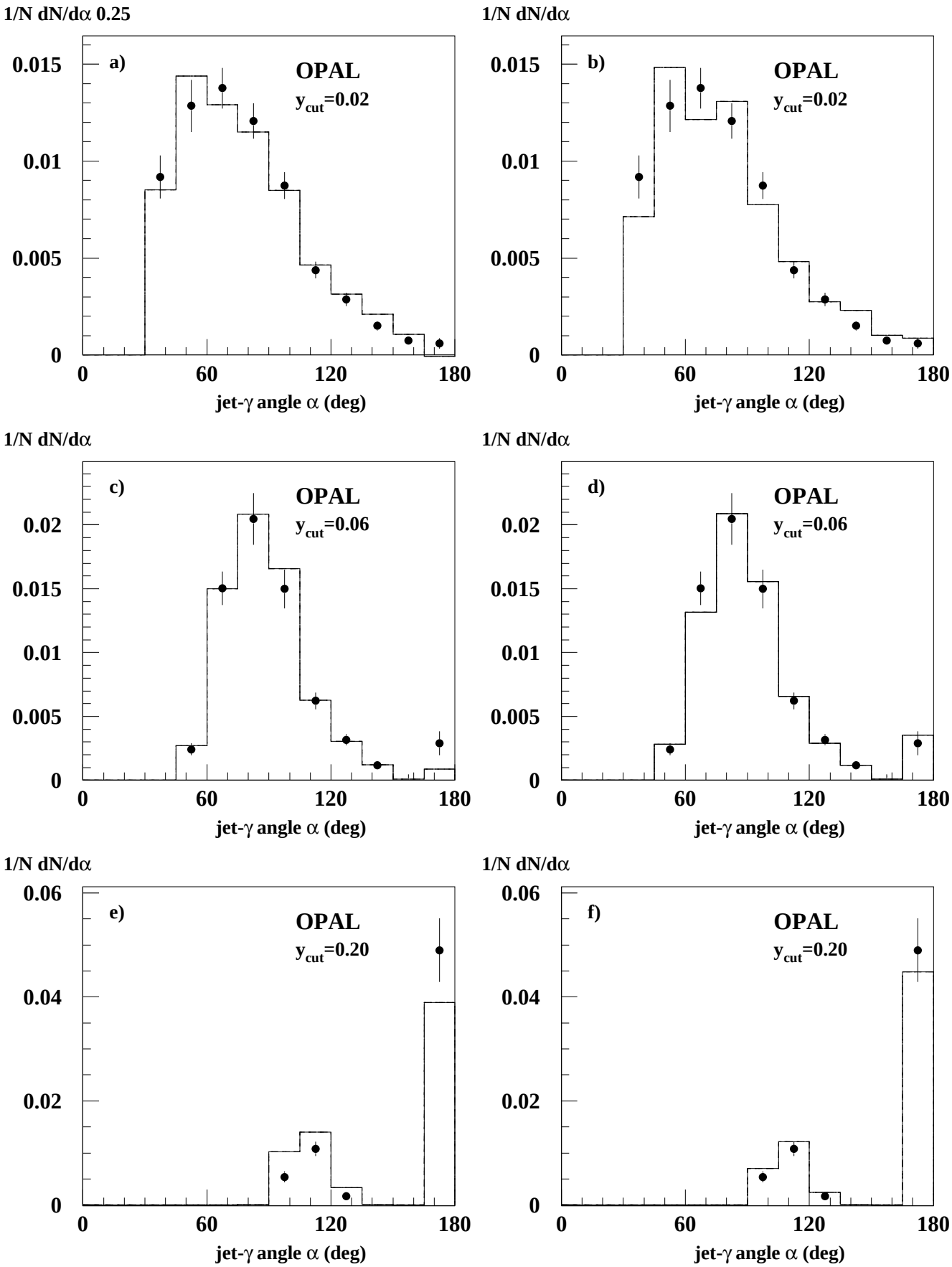
EEPRAD
GNJETS
1/N dN/dα 0.25
1/N dN/dα
a)
b)
c)
d)
e)
f)
OPAL
y_{cut}=0.02
y_{cut}=0.06
y_{cut}=0.20
0.015
0.01
0.005
0
0.02
0.04
0.06
0
60
120
180
jet-γ angle α (deg)

Figure 6

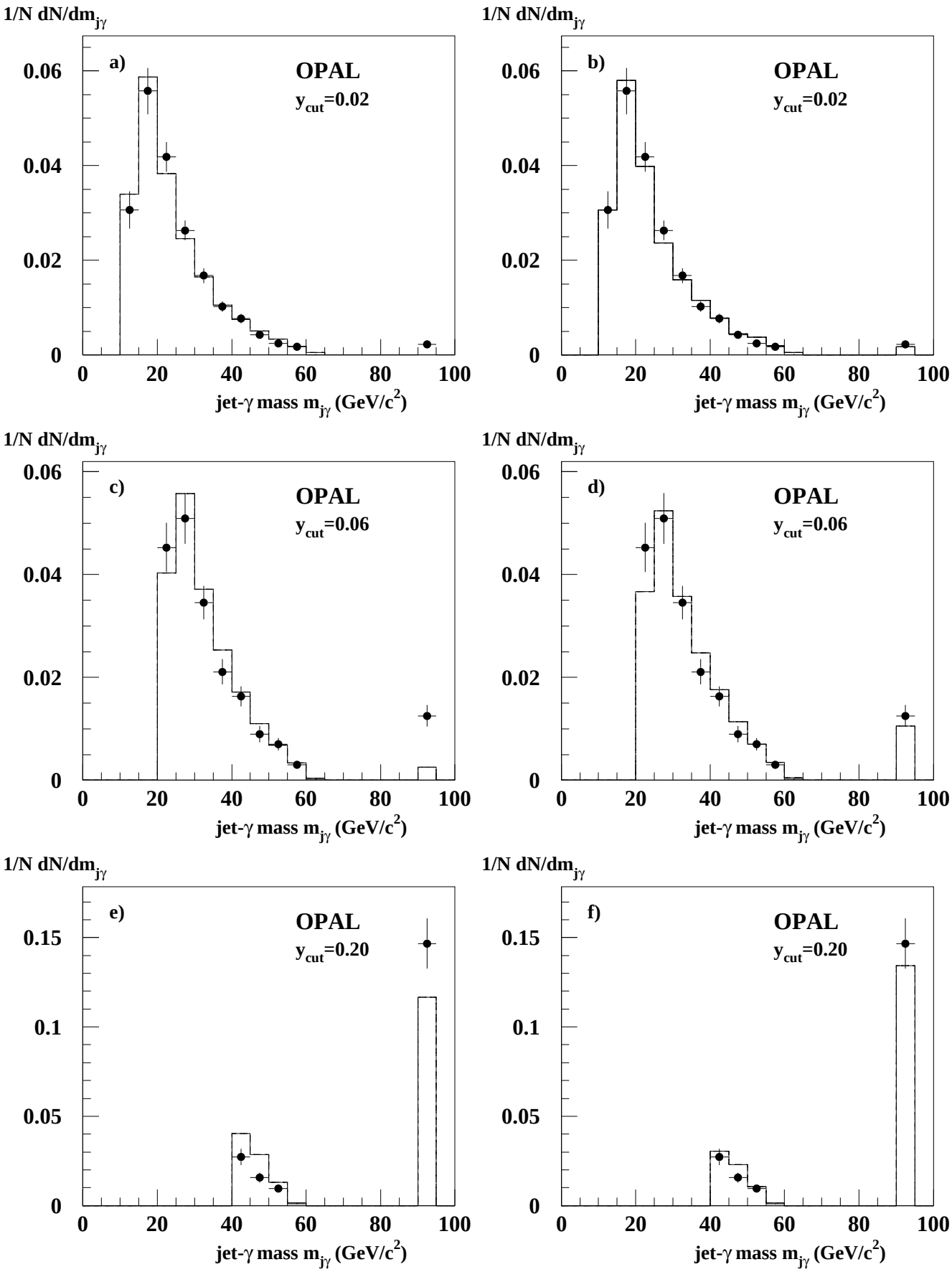
EEPRAD
GNJETS
1/N dN/dm$_{j\gamma}$
a)
b)
c)
d)
e)
f)
OPAL
y_{cut}=0.02
y_{cut}=0.06
y_{cut}=0.20
jet-γ mass $m_{j\gamma}$ (GeV/c^2)
0
0.02
0.04
0.06
0.05
0.1
0.15
0
20
40
60
80
100

Figure 7